

Computing steady-state solutions for a free boundary problem modeling tumor growth by Stokes equation

Wenrui Hao* Jonathan D. Hauenstein† Bei Hu‡
Timothy McCoy§ Andrew J. Sommese¶

August 29, 2011

Abstract

We consider a free boundary problem modeling tumor growth where the model equations include a diffusion equation for the nutrient concentration and the Stokes equation for the proliferation of tumor cells. For any positive radius R , it is known that there exists a unique radially symmetric stationary solution. The proliferation rate μ and the cell-to-cell adhesiveness γ are two parameters for characterizing “aggressiveness” of the tumor. We compute symmetry-breaking bifurcation branches of solutions by studying a polynomial discretization of the system. By tracking the discretized system, we numerically verified a sequence of μ/γ symmetry breaking bifurcation branches. Furthermore, we study the stability of both radially symmetric and radially asymmetric stationary solutions.

*Department of Applied and Computational Mathematics and Statistics, University of Notre Dame, Notre Dame, IN 46556 (whao@nd.edu). This author was supported by the Dunces Chair of the University of Notre Dame and NSF grant DMS-0712910.

†Department of Mathematics, Mailstop 3368, Texas A&M University, College Station, TX 77843 (jhauenst@math.tamu.edu, www.math.tamu.edu/~jhauenst). This author was supported by Texas A&M University and NSF grant DMS-0915211 and DMS-1114336.

‡Department of Applied and Computational Mathematics and Statistics, University of Notre Dame, Notre Dame, IN 46556 (b1hu@nd.edu, www.nd.edu/~b1hu).

§Department of Applied and Computational Mathematics and Statistics, University of Notre Dame, Notre Dame, IN 46556 (tmccoy@nd.edu).

¶Department of Applied and Computational Mathematics and Statistics, University of Notre Dame, Notre Dame, IN 46556 (sommese@nd.edu, www.nd.edu/~sommese). This author was supported by the Duncan Chair of the University of Notre Dame and NSF grant DMS-0712910.

Keywords: Free boundary problems; Stationary solution; Stokes equation; Bifurcation; Stability; Homotopy continuation; Tumor growth

1 Introduction

Mathematical models of tumor growth, which consider the tumor tissue as a density of proliferating cells, have been developed and studied in many papers; see [1, 3, 5, 6, 7, 8, 9, 15, 17] and their references. These models treat tumor tissue as a porous medium described by Darcy's law. However, there are tumors for which the tissue is more naturally modeled as a fluid. For example, in the early stages of breast cancer, the tumor is confined to the duct of a mammary gland, which consists of epithelial cells, a meshwork of proteins, and mostly extracellular fluid. Several papers on ductal carcinoma in the breast use the Stokes equation in their mathematical models [10, 11, 12] with a focus on the radially symmetric case since tumors grown in vitro have a nearly spherical shape, it is important to determine whether these radially symmetric tumors are asymptotically stable. While tumors grown in vitro have a nearly spherical shape, tumors grown in vivo are usually not. It is therefore also interesting to study what will happen for the radially asymmetric tumors.

Let $\Omega(t)$ denote the tumor domain at time t , and p be the pressure within the tumor resulting from proliferation of the tumor cells. The density of the cells, c , depends on the concentration of nutrients, σ , and assuming that this dependence is linear, we may simply identify c with σ . We also assume the proliferation rate, S , depends linearly upon σ . That is,

$$\operatorname{div} \vec{v} = S = \mu(\sigma - \tilde{\sigma}) \quad \text{in } \Omega(t), \quad (1)$$

where $\tilde{\sigma} > 0$ is a threshold concentration and μ is the proliferation rate which expresses the "intensity" of the expansion or shrinkage. The first order Taylor expansion for the fully nonlinear model yields the linear approximation $\mu(\sigma - \tilde{\sigma})$ used here.

If we assume that the consumption rate of nutrients is proportional to the concentration of the nutrients, then after normalization, σ satisfies

$$\sigma_t - \Delta \sigma = -\sigma \quad \text{in } \Omega(t) \quad \text{and} \quad \sigma = 1 \quad \text{on } \partial\Omega(t). \quad (2)$$

Most tumor models assume that the tissue has the structure of a porous medium so that Darcy's law holds. In particular, $\vec{v} = -\nabla p$ where \vec{v} is the

velocity of the cells and p is the pressure. However, the tissue is modeled as a fluid in the current model. In this case, the stress tensor is given by $\sigma_{ij} = -p\delta_{ij} + 2\nu\left(e_{ij} - \frac{1}{3}\bar{\Delta}\delta_{ij}\right)$ where $p = -\frac{1}{3}\sum_{k=1}^3\sigma_{kk}$, ν is the viscosity coefficient, $e_{ij} = \frac{1}{2}\left(\frac{\partial v_i}{\partial x_j} + \frac{\partial v_j}{\partial x_i}\right)$ is the strain tensor, δ is the Kronecker delta and $\bar{\Delta} = \sum_{k=1}^3 e_{kk} = \text{div}\vec{v}$ is the dilation. If there are no body forces, then $\sum_{j=1}^3 \frac{\partial \sigma_{ij}}{\partial x_j} = 0$ which can be written as the Stokes equation

$$-\nu\Delta\vec{v} + \nabla p - \frac{1}{3}\nu\nabla\text{div}\vec{v} = 0 \quad \text{in } \Omega(t), \quad t > 0. \quad (3)$$

Assuming that the strain tensor is continuous up to the boundary of the domain, we then obtain a boundary condition:

$$T\vec{n} = -\gamma\kappa\vec{n} \quad \text{on } \partial\Omega(t), \quad t > 0, \quad (4)$$

where T is the stress tensor: $T = \nu(\nabla\vec{v} + (\nabla\vec{v})^T) - (p + \frac{2}{3}\nu\text{div}\vec{v})I$ with components

$$T_{ij} = \nu\left(\frac{\partial v_i}{\partial x_j} + \frac{\partial v_j}{\partial x_i}\right) - \delta_{ij}\left(p + \frac{2\nu}{3}\text{div}\vec{v}\right),$$

where \vec{n} is the outward normal, κ is the mean curvature, and γ is the cell-to-cell adhesiveness constant.

The free boundary condition is given by the kinematic condition

$$V_n(t) = \vec{v} \cdot \vec{n} \quad \text{on } \partial\Omega(t). \quad (5)$$

Summarizing these equations, we obtain

$$\left\{ \begin{array}{ll} \sigma_i - \Delta\sigma + \sigma = 0 & \text{in } \Omega(t) \\ -\Delta\vec{v} + \nabla p = (\mu/3)\nabla(\sigma - \tilde{\sigma}) & \text{in } \Omega(t) \\ \text{div}\vec{v} = \mu(\sigma - \tilde{\sigma}) & \text{in } \Omega(t) \\ T(\vec{v}, p)\vec{n} = (-\gamma\kappa + \frac{2\nu}{3}\mu(1 - \tilde{\sigma}))\vec{n} & \text{on } \partial\Omega(t) \\ \sigma = 1 & \text{on } \partial\Omega(t) \\ \vec{v} \cdot \vec{n} = V_n & \text{on } \partial\Omega(t) \\ \int_{\Omega(t)} \vec{v} dx = 0, \quad \int_{\Omega(t)} \vec{v} \times \vec{x} dx = 0 & \end{array} \right. \quad (6)$$

where the last two conditions represent the choice of a coordinate system that excludes the six-dimensional kernel of (1), (3) and (4), which consists of rigid motions.

The steady state fluid-like tumor system is [13]:

$$\left\{ \begin{array}{ll} -\Delta\sigma + \sigma = 0 & \text{in } \Omega \\ -\Delta\vec{v} + \nabla p = (\mu/3)\nabla(\sigma - \tilde{\sigma}) & \text{in } \Omega \\ \operatorname{div}\vec{v} = \mu(\sigma - \tilde{\sigma}) & \text{in } \Omega \\ T(\vec{v}, p)\vec{n} = (-\gamma\kappa + \frac{2\mu}{3}\mu(1 - \tilde{\sigma}))\vec{n} & \text{on } \partial\Omega \\ \sigma = 1 & \text{on } \partial\Omega \\ \vec{v} \cdot \vec{n} = 0 & \text{on } \partial\Omega \\ \int_{\Omega} \vec{v} dx = 0 \quad , \quad \int_{\Omega} \vec{v} \times \vec{x} dx = 0 & \end{array} \right. \quad (7)$$

where $T(\vec{v}, p)\vec{n} = (\nabla\vec{v})^T + \nabla\vec{v} - pI$ with I the 3×3 identity matrix.

In [13], it is proved that there exists a unique radially symmetric solution with free boundary $r = R$ for any given positive number R . For a sequence $\mu/\gamma = M_n(R)$ there exist symmetry-breaking bifurcation branches of solutions with boundary $r = R + \epsilon Y_{n,0}(\theta) + O(\epsilon^2)$ (n even ≥ 2) for small $|\epsilon|$, where $Y_{n,0}$ is the spherical harmonic of mode $(n, 0)$. Note that these results are valid only in a small neighborhood of the bifurcation branching point. In this paper, we use the numerical method presented in [16] to find the radially asymmetric solutions as the parameters *go beyond this small neighborhood*, e.g., Figure 4. Compare with the system in [16], this system has more variables and increased complexity when using a similar discretization scheme. This required us to implement and use parallel differentiation and a sparse linear solver in order to perform the large-scale numerical computations needed for the method developed in [16].

2 Discretization

We use the same grid and scheme in [16] for the spherical coordinate expression of the radially symmetric stationary solution of system (7) presented in [13]. The formula for the operators in the system in spherical coordinates is deduced in the Appendix. The values (σ, \vec{v}, p) in the small neighborhood of a bifurcation point obtained in [13] via linearization are

$$\left\{ \begin{array}{l} \sigma = \sigma_s + \epsilon\sigma_1 + O(\epsilon^2), \quad \sigma_1 = -(\sigma_s)_r(R) \frac{I_{l+1/2}(r)}{r^{1/2}} \frac{R^{1/2}}{I_{l+1/2}(R)} Y_{l,0}(\theta, \phi) \\ p = p_s + \epsilon p_1 + O(\epsilon^2), \quad p_1 = \frac{4\mu}{3}\sigma_1 + p_{l,0}(r) Y_{l,0}(\theta, \phi) \\ \vec{v} = \vec{v}_s + \epsilon\vec{v}_1 + O(\epsilon^2), \quad \vec{v}_1 = \vec{a} + \vec{b} \times \vec{x} + H_1(r) Y_{l,0} \vec{e}_r + H_2(r) \nabla_{\omega} Y_{l,0}(\theta, \phi) \end{array} \right. ,$$

where $Y_{l,0}(\theta, \phi)$ is the spherical harmonic function, which satisfies $Y_{l,0}(\theta, \phi) = Y_{l,0}(\pi - \theta, \phi)$, and $H_1(r), H_2(r)$ are functions of r (see [13] for detail). Then

Tumor Model	N_θ	N_R	Number of variables	time
porous media in [16]	16	30	575	8m24s
	32	60	1135	1h30m
fluid-like	16	30	1008	7h28m
	32	60	3938	26h34m

Table 1: Comparison of polynomial system solving times

σ and p are symmetric with respect to $\frac{\pi}{2}$. We note that \vec{v} can be written as $v_r\vec{e}_r + v_\theta\vec{e}_\theta + v_\phi\vec{e}_\phi$, that $\nabla_\omega = \frac{1}{\sin(\theta)}\frac{\partial}{\partial\theta}\left(\sin(\theta)\frac{\partial}{\partial\theta}\right) + \frac{1}{\sin^2\theta}\frac{\partial^2}{\partial\phi^2}$, and

$$\begin{cases} \sigma(\theta) = \sigma(\pi - \theta) \\ p(\theta) = p(\pi - \theta) \\ v_r(\theta) = v_r(\pi - \theta) \\ v_\phi(\theta) = 0 \\ -v_\theta(\theta) = v_\theta(\pi - \theta) \end{cases} \quad \text{for } \theta \in \left[0, \frac{\pi}{2}\right]$$

for the bifurcation branch of $M_n(R)$, where n is an even number. In particular, due to this symmetry, we can construct the grid points on one-eighth of the domain and then extend using symmetry to yield solutions to the whole domain.

3 Bifurcation of $M_n(R)$

Using the floating grid and third order scheme presented in [16], we setup a discretization of the system (7) yielding a polynomial system. Due to the complexity of this polynomial system, it required more computational power than the tumor system in [16]. We used Bertini [2] to handle this polynomial system running on a Xeon 5410 processor using 64-bit Linux. In order to better handle this large-scale problem using Bertini, we implemented parallel differentiation and a sparse linear algebra solver based on BLAS [4] in Bertini. Table 1 compares the number of variables and time needed to track the discretized polynomial systems along the radially symmetric branch between porous media tumor model and fluid-like tumor model. In this table, N_θ and N_R denote the number of grid points in the angular and radial directions, respectively.

n	formula [13]	numerical value
M_4	0.47481	0.47494
M_6	0.47629	0.47702

Table 2: Comparison of the numerical values of μ_n with the actual value for a radius of $R = 12.5$

The system is parameterized by μ and γ , which characterize the “aggressiveness” of the tumor. It is known [13] that there exists a unique radially symmetric solution with any given μ . When we are tracking the radially symmetric solutions along the parameter μ with $\gamma = 1$, the Jacobian will become singular at μ_n where there exists a bifurcation. Starting from a radially symmetric solution and using parameter continuation with respect to μ , we are able to compute the value of M_n numerically. Figure 1 plots the condition number of radially symmetric solutions for different μ ranging between $\mu = 0.47$ and $\mu = 0.48$ with $R = 12.5$. We note that this figure shows that there are two bifurcations, namely $\mu = M_4$ and $\mu = M_6$, respectively. Table 2 compares the numerically computed values of M_n with the values of M_n given by the symbolic formulas derived in [13].

The radially asymmetric solutions along the bifurcation branches are even more interesting. We found that the double precision arithmetic in Matlab was unable to accurately compute the tangent directions at μ_n . This stems from the fact that the Jacobian matrix is singular at μ_n and has condition number around 10^9 even at values of μ where it is nonsingular. By using multiprecision arithmetic implemented in Bertini [2], we were able to compute the tangent directions which agreed with the symbolic formulas derived in [14]. Upon computing the tangent direction, we utilized parameter continuation to track the radially asymmetric solution branches passing through the values of M_4 and M_6 computed above. Figure 2 shows the solution behavior of these branches which were computed using $N_R = 60$ grid points in the radial direction and $N_\theta = 32$ grid points in the angular direction. The function $\epsilon(\theta)$ in this figure is defined in [16] allowing us to plot the branches. By looking at Figure 2, we see that there are three intersections. The two intersection, denoted M_U and M_L in Figure 2 are self-intersections which arise simply by the choice of the projection since the corresponding nonradial solutions as these points are distinct. The intersection denoted $M_{\text{nonradial}}$ in Figure 2 is indeed a nonradial bifurcation. To demonstrate this, Figure 3

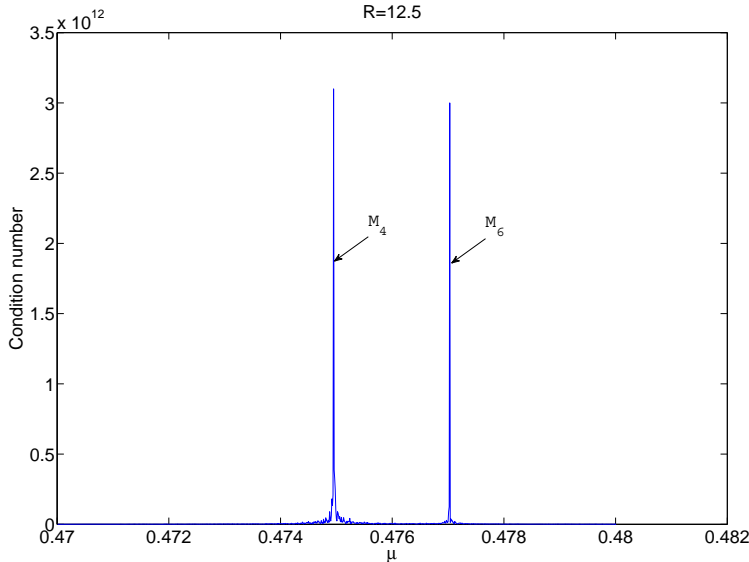


Figure 1: Condition Number of the radially symmetric solution vs. μ

plots the condition number along this path and clearly shows a bifurcation corresponding to the point $M_{\text{nonradial}}$. Figure 4 plots two nonradial solutions lying on the M_4 and M_6 branches, respectively

4 Homotopy continuation of M_n to R

For the porous medium tissue model, the smallest value of μ/γ which generates protrusions is $M_2(R)$. At this point, the tumor will have just three protrusions independent of the value of R . However, in the case of a fluid-like tissue, [14] shows that the smallest value of μ/γ which generates protrusions is $M_{n^*}(R)$, where n^* depends on R . Therefore, one natural question is to determine the values of R where n^* changes.

Since the value of $M_n(R)$ corresponds with a singular solution of a polynomial system, we use deflation to construct a new polynomial system which allows us to track along the path $M_n(R)$ parameterized by R . Let $f(x, \mu)$ denote the discretized polynomial system, where x^* corresponds to the numerical solution (σ, p, \vec{v}) at the bifurcation point μ^* of interest. Let $Jf(x, \mu)$

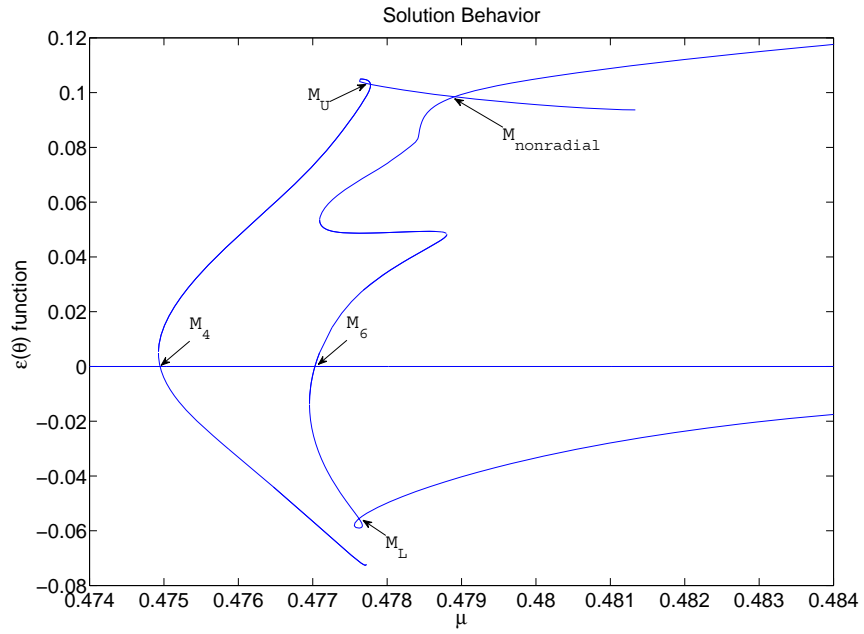


Figure 2: Solution Behavior

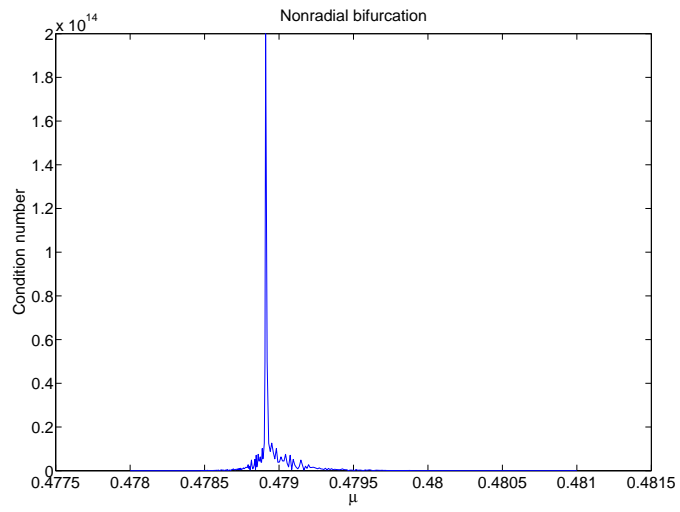


Figure 3: Nonradial bifurcation

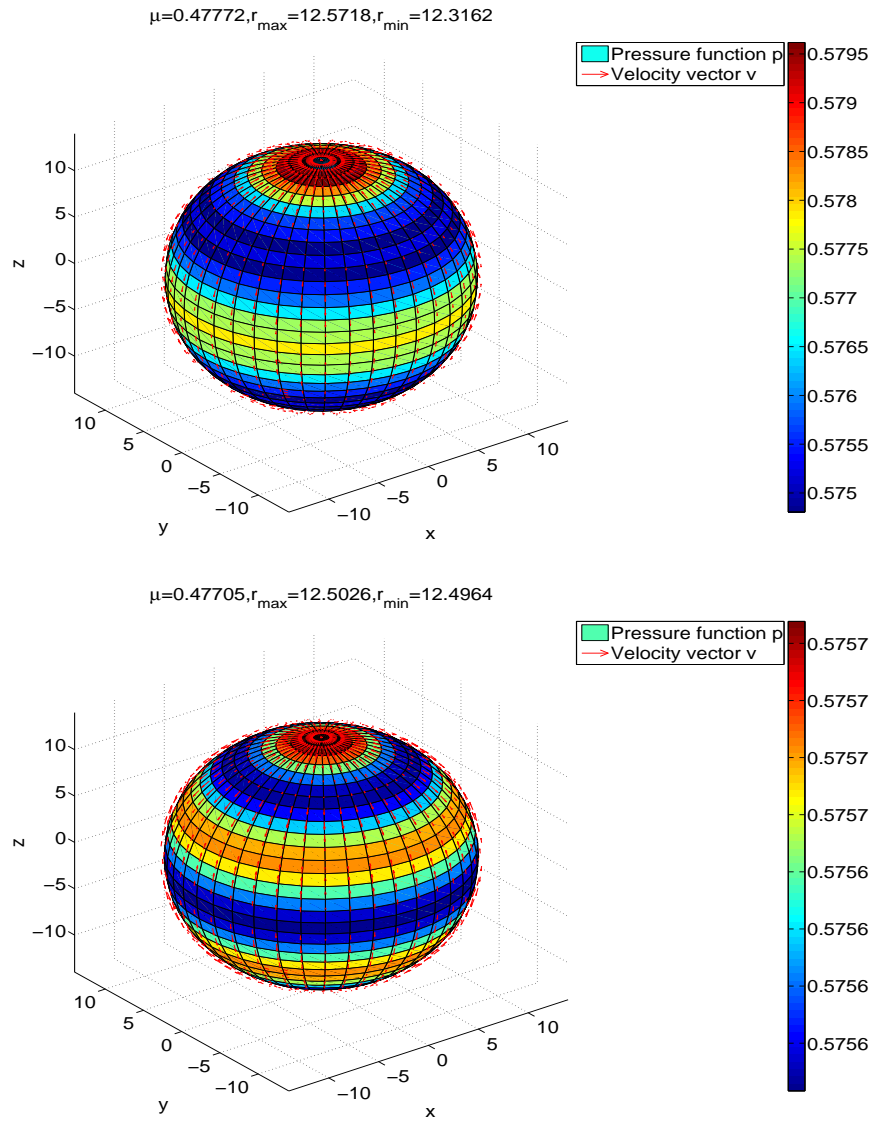


Figure 4: Radially asymmetric solutions

be the Jacobian matrix of f at x . Since the Jacobian is rank deficient, it has nonzero null vectors. One step of the deflation process adds polynomials to f to yield a general element in this null space, namely the polynomial system

$$g(x, \mu, \xi) = \begin{bmatrix} f(x, \mu) \\ Jf(x, \mu)\xi \\ \mathcal{L}(\xi) \end{bmatrix}$$

where $\mathcal{L}(\xi)$ is a general linear system so that there is a unique value of ξ such that $g(x^*, \mu^*, \xi) = 0$. Using this augmented polynomial system, we can track a bifurcation value M_n as R varies. Figure 5 plots the value of M_4 with respect to R along with the numerical error. At the values R^* where n^* changes, the solution (x, μ, ξ) is singular, that is, the Jacobian matrix of $g(x, \mu, \xi)$ is rank deficient. Figure 6 plots the condition number of $Jg(x, \mu, \xi)$ with respect to R . This computation yields a numerical value of $R^* = 12.8778$.

5 Linear stability

We now turn our attention to the numerical determination of solution stability. In order to check linear stability, we rewrite (6) as

$$u_t = F(u, \mu, \tilde{\sigma}, \gamma),$$

where $u = (r, \sigma, p, \vec{v})$, r is the function of the angle θ describing the boundary and $F(u, \mu, \tilde{\sigma}, \gamma)$ represents the steady state system (7). The linearization of the system (6) gives

$$u(t) = u_0 + \epsilon u_1(t) + O(\epsilon^2), \quad (8)$$

where u_0 is the steady state solution. Substituting (8) into (6), we have

$$\begin{aligned} & \left(u_0 + \epsilon u_1(t) + O(\epsilon^2) \right)_t = F(u_0 + \epsilon u_1(t) + O(\epsilon^2), \mu, \tilde{\sigma}, \gamma) \\ \Rightarrow & (u_0)_t + \epsilon (u_1)_t + O(\epsilon^2) = F(u_0, \mu, \tilde{\sigma}, \gamma) + JF(u_0, \mu, \tilde{\sigma}, \gamma)u_1\epsilon + O(\epsilon^2) \\ \Rightarrow & (u_1)_t = JF(u_0, \mu, \tilde{\sigma}, \gamma)u_1, \end{aligned} \quad (9)$$

where $JF(u_0, \mu, \tilde{\sigma}, \gamma)$ is the Jacobian of $F(u, \mu, \tilde{\sigma}, \gamma)$ at u_0 . Let U_1^n denote the numerical approximation of $u_1(n\tau)$, where τ is the time step size. Then the discretization of (9) leads to

$$U_1^{n+1} = (I - JF(u_0, \mu, \tilde{\sigma}, \gamma)\tau)^{-1}U_1^n \doteq AU_1^n,$$

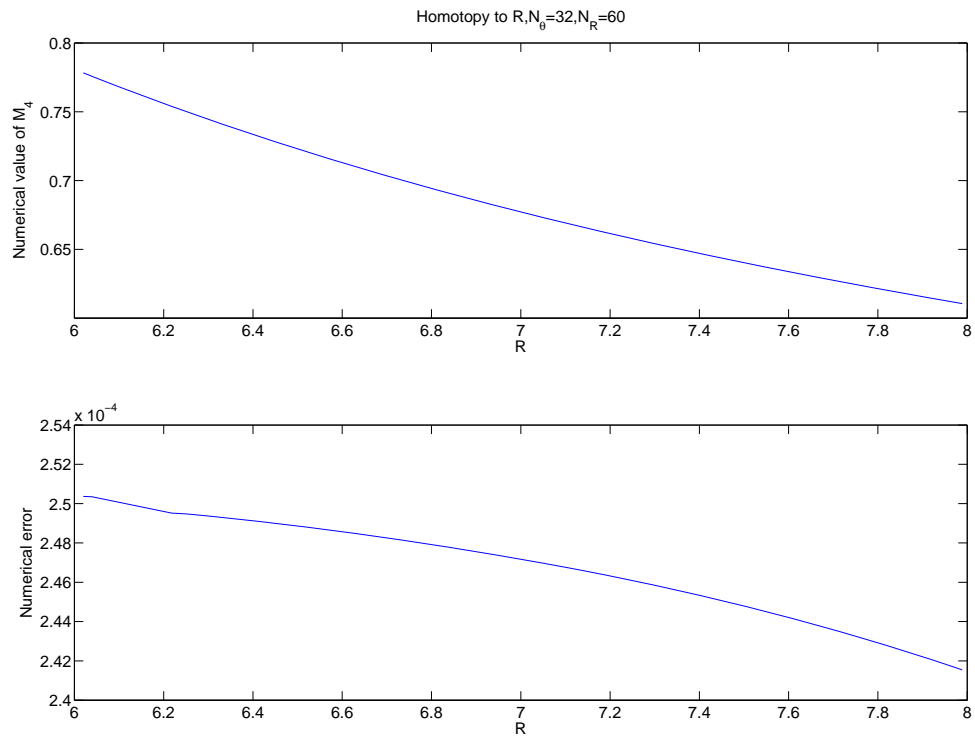


Figure 5: Homotopy of M_4

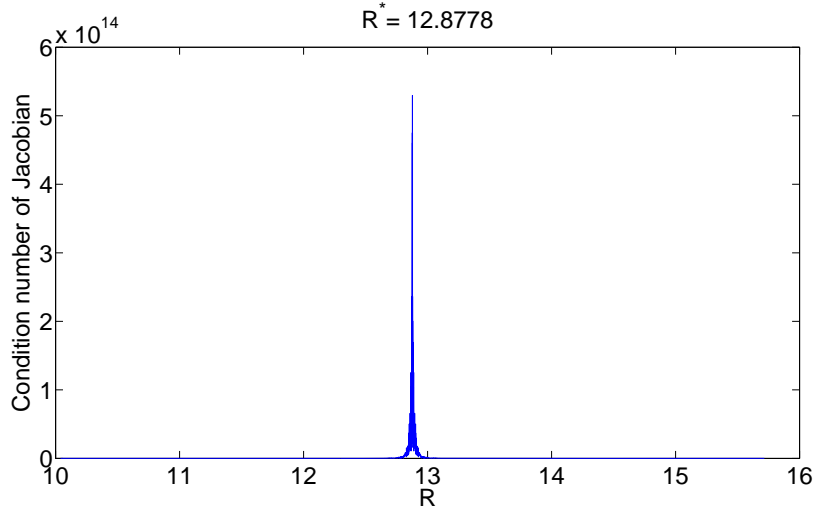


Figure 6: Condition number of $Jg(x, \mu, \xi)$ v.s. R

where I is the identity matrix. This process transfers the linear stability to the spectrum of A . Let $|\rho(A)|$ denote the maximum of the absolute values of the eigenvalues of A . If $|\rho(A)| < 1$, then $\|U_1^n\| \rightarrow 0$ yielding a stable system. The system is unstable if $|\rho(A)| > 1$. Continuing with the working example described in Section 3, namely $R = 12.5$, we computed the eigenvalues of A for different values of μ along the radially asymmetric solution branches to determine the stability which are displayed in Table 3. We note that “U” and “L” represent the “upper” and “lower” branches, respectively.

Table 3 shows that the solution is unstable even before the parameter μ reaches its first bifurcation point. This is in contrast with tumors growing in porous media environment where spherical instability occurs only when μ reaches the first bifurcation point. Moreover, all of the nonradial solutions computed are unstable while there are some stable nonradial solutions for a porous tumor [16].

Acknowledgement

We would like to thank the Notre Dame Center for Research Computing (crc.nd.edu) for their help. Not only for helping maintain our group’s com-

Table 3: Maximum eigenvalue for different values of μ

Radial branch		M_4 nonradial branch		M_6 nonradial branch	
μ	$ \rho(A) $	μ	$ \rho(A) $	μ	$ \rho(A) $
1e-2	9.98647e-1	4.75766e-1U	1.00013	4.76956e-1U	1.00013
5e-2	9.99898e-1	4.76641e-1U	1.00026	4.77128e-1U	1.00014
1e-1	9.99996e-1	4.78324e-1U	1.00034	4.77297e-1U	1.00017
2e-1	1.00032	4.79012e-1U	1.00057	4.78802e-1U	1.00024
3e-1	1.00012	4.82764e-1U	1.00106	4.79208e-1U	1.00039
4e-1	1.00049	4.75766e-1L	1.00010	4.77093e-1L	1.00014
5e-1	1.00148	4.76000e-1L	1.00017	4.78053e-1L	1.0026
6e-1	1.00638	4.76290e-1L	1.00022	4.78727e-1L	1.0046
8e-1	1.01846	4.77101e-1L	1.00027	4.82026e-1L	1.0098
1	1.09861	4.77629e-1L	1.00032	4.84000e-1L	1.0147

puter cluster, but for providing access to a high memory node during the period when we were parallelizing the differentiation code in Bertini.

References

- [1] J. A. ADAM AND S. A. MAGGELAKIS, Diffusion regulated growth characteristics of a spherical prevascular carcinoma, *Bull. Math. Biol.*, Vol. 52, pp. 549–582. (1990)
- [2] D.J. BATES, J.D. HAUENSTEIN, A.J. SOMMESE, AND C.W. WAMPLER, Bertini: Software for numerical algebraic geometry. *Available at www.nd.edu/~sommese/bertini*.
- [3] N. BRITTON AND M.A.J. CHAPLAIN, A qualitative analysis of some models of tissue growth, *Math. Biosci.*, Vol. 113, pp. 77–89, (1993).
- [4] Sparse Basic Linear Algebra Subprograms (BLAS) Library, <http://math.nist.gov/spblas/>.
- [5] H.M. BYRNE, The importance of intercellular adhesion in the development of carcinomas, *IMA J. Math. Appl. Med. Biol.*, Vol. 14, pp. 305–323, (1997).

- [6] H.M. BYRNE, A weakly nonlinear analysis of a model of avascular solid tumor growth, *J. Math. Biol.*, Vol. 39, pp. 59–89, (1999).
- [7] H.M. BYRNE AND M.A.J. CHAPLAIN, Growth of nonnecrotic tumors in the presence and absence of inhibitors, *Math. Biosci.*, Vol. 130, pp. 151–181, (1995).
- [8] H.M. BYRNE AND M.A.J. CHAPLAIN, Modelling the role of cell-cell adhesion in the growth and development of carcinomas, *Mathl. Comput. Modelling*, Vol. 12, pp. 1–17, (1996).
- [9] M.A.J. CHAPLAIN, The development of a spatial pattern in a model for cancer growth, *Experimental and Theoretical Advances in Biological Pattern Formation* (H.G. Othmer, P.K. Maini, and J.D. Murray, eds), Plenum Press, pp. 45–60, (1993).
- [10] S.J.H. FRANKS, H.M. BYRNE, J.C.E. UNDERWOOD AND C.E. LEWIS, Biological inferences from a mathematical model of comedo ductal carcinoma in situ of the breast, *J. Theoretical Biology* Vol. 232, pp. 523–543, (2005).
- [11] S.J.H. FRANKS, H.M. BYRNE, J.P. KING, J.C.E. UNDERWOOD AND C.E. LEWIS, Modelling the early growth of ductal carcinoma in situ of the breast, *J. Math. Biology*, Vol. 47, pp. 424–452. (2003)
- [12] S.J.H. FRANKS, H.M. BYRNE, J.P. KING, J.C.E. UNDERWOOD AND C.E. LEWIS, Modelling the growth of ductal carcinoma in situ, *Mathematical Medicine & Biology*, Vol. 20, pp. 277–308, (2003).
- [13] A. FRIEDMAN AND B. HU, Bifurcation for a free boundary problem modeling tumor growth by stokes equation *SIAM J. Math. Anal.*, Vol. 30, No. 1, pp.174–194, (2006).
- [14] A. FRIEDMAN AND B. HU, Bifurcation from stability to instability for a free boundary problem modeling tumor growth by stokes equation, *J. Math. Anal. Appl.* Vol. 207, pp. 643–664, (2007).
- [15] H. P. GREENSPAN, On the growth of cell culture and solid tumors, *J. Theoret. Biol.*, Vol. 56, pp. 229–242, (1976).

- [16] W. HAO, J.D. HAUENSTEIN, B. HU AND A.J. SOMMESE, A three-dimensional steady-state tumor system, *Appl. Math. Comp.*, to appear.
- [17] D.L.S. MCEWAIN AND L.E. MORRIS, Apoptosis as a volume loss mechanism in mathematical models of solid tumor growth, *Math. Biosci.*, Vol. 39, 147–157, (1978).

Appendix: Operators under the spherical coordinate

We use the notation $\vec{e}_r, \vec{e}_\theta, \vec{e}_\phi$ for the unit normal vectors in the r, θ, ϕ directions, respectively; here $0 \leq r \leq \infty$, $0 \leq \theta \leq \pi$, $0 \leq \phi \leq 2\pi$. Then, written in Cartesian coordinates in \mathbb{R}^3 ,

$$\begin{aligned}\vec{e}_r &= \vec{e}_1 \sin \theta \cos \phi + \vec{e}_2 \sin \theta \sin \phi + \vec{e}_3 \cos \theta, \\ \vec{e}_\theta &= \vec{e}_1 \cos \theta \cos \phi + \vec{e}_2 \sin \theta \sin \phi + \vec{e}_3 \cos \theta, \\ \vec{e}_\phi &= -\vec{e}_1 \sin \phi + \vec{e}_2 \cos \phi,\end{aligned}$$

where $(\vec{e}_1, \vec{e}_2, \vec{e}_3)$ is the standard basis in \mathbb{R}^3 in Cartesian coordinates.

The gradient of the vector $\nabla \vec{v}$, where $\vec{v} = (v_r, v_\theta, v_\phi)^T = v_r \vec{e}_r + v_\theta \vec{e}_\theta + v_\phi \vec{e}_\phi$, is given by

$$\nabla \vec{v} = \nabla v_r \otimes \vec{e}_r + \nabla v_\theta \otimes \vec{e}_\theta + \nabla v_\phi \otimes \vec{e}_\phi + v_r \nabla \vec{e}_r + v_\theta \nabla \vec{e}_\theta + v_\phi \nabla \vec{e}_\phi. \quad (10)$$

In polar spherical coordinates, the gradient of a function f has the following form:

$$\nabla f = \frac{\partial f}{\partial r} \vec{e}_r + \frac{1}{r \sin \theta} \frac{\partial f}{\partial \phi} \vec{e}_\phi + \frac{1}{r} \frac{\partial f}{\partial \theta} \vec{e}_\theta.$$

Then, we can deduce the each term of (10) as follows,

$$\begin{aligned}
\nabla v_r \otimes \vec{e}_r &= \left(\frac{\partial v_r}{\partial r} \vec{e}_r + \frac{1}{r \sin \theta} \frac{\partial v_r}{\partial \phi} \vec{e}_\phi + \frac{1}{r} \frac{\partial v_r}{\partial \theta} \vec{e}_\theta \right) \otimes \vec{e}_r \\
&= \frac{\partial v_r}{\partial r} \vec{e}_r \otimes \vec{e}_r + \frac{1}{r \sin \theta} \frac{\partial v_r}{\partial \phi} \vec{e}_\phi \otimes \vec{e}_r + \frac{1}{r} \frac{\partial v_r}{\partial \theta} \vec{e}_\theta \otimes \vec{e}_r \\
\nabla v_\theta \otimes \vec{e}_\theta &= \frac{\partial v_\theta}{\partial r} \vec{e}_r \otimes \vec{e}_\theta + \frac{1}{r \sin \theta} \frac{\partial v_\theta}{\partial \phi} \vec{e}_\phi \otimes \vec{e}_\theta + \frac{1}{r} \frac{\partial v_\theta}{\partial \theta} \vec{e}_\theta \otimes \vec{e}_\theta \\
\nabla v_\phi \otimes \vec{e}_\phi &= \frac{\partial v_\phi}{\partial r} \vec{e}_r \otimes \vec{e}_\phi + \frac{1}{r \sin \theta} \frac{\partial v_\phi}{\partial \phi} \vec{e}_\phi \otimes \vec{e}_\phi + \frac{1}{r} \frac{\partial v_\phi}{\partial \theta} \vec{e}_\theta \otimes \vec{e}_\phi \\
v_r \nabla \vec{e}_r &= v_r \left(\frac{\partial \vec{e}_r}{\partial r} \vec{e}_r + \frac{1}{r \sin \theta} \frac{\partial \vec{e}_r}{\partial \phi} \vec{e}_\phi + \frac{1}{r} \frac{\partial \vec{e}_r}{\partial \theta} \vec{e}_\theta \right) \\
&= \frac{v_r}{r} (\vec{e}_\phi \otimes \vec{e}_\phi + \vec{e}_\theta \otimes \vec{e}_\theta) \\
v_\theta \nabla \vec{e}_\theta &= \frac{v_\theta}{r} (\cot \theta \vec{e}_\phi \otimes \vec{e}_\phi - \vec{e}_r \otimes \vec{e}_\theta) \\
v_\phi \nabla \vec{e}_\phi &= -\frac{v_\phi}{r} (\cot \theta \vec{e}_\theta \otimes \vec{e}_\phi + \vec{e}_r \otimes \vec{e}_\phi)
\end{aligned}$$

Therefore, we summarize the gradient of velocity as

$$\nabla \vec{v} = \begin{pmatrix} \frac{\partial v_r}{\partial r}, & \frac{1}{r} \frac{\partial v_r}{\partial \theta}, & \frac{1}{r \sin \theta} \frac{\partial v_r}{\partial \phi} \\ \frac{\partial v_\theta}{\partial r} - \frac{v_\theta}{r}, & \frac{1}{r} \frac{\partial v_\theta}{\partial \theta} + \frac{v_r}{r}, & \frac{1}{r \sin \theta} \frac{\partial v_\theta}{\partial \phi} \\ \frac{\partial v_\phi}{\partial r} - \frac{v_\phi}{r}, & \frac{1}{r} \frac{\partial v_\phi}{\partial \theta} - \frac{\cot \theta}{r} v_\phi, & \frac{1}{r \sin \theta} \frac{\partial v_\phi}{\partial \phi} + \frac{v_r}{r} + \frac{\cot \theta}{r} v_\theta \end{pmatrix}.$$

A vector Laplacian can be defined for a vector \vec{v} by

$$\Delta \vec{v} = \nabla(\nabla \cdot \vec{v}) - \nabla \times (\nabla \times \vec{v}).$$

Moreover, the curl $\nabla \times \vec{v}$ under spherical coordinates is given by

$$\nabla \times \vec{v} = \frac{\vec{e}_r}{r \sin \theta} \left[\frac{\partial}{\partial \theta} (v_\phi \sin \theta) - \frac{\partial v_\theta}{\partial \phi} \right] + \frac{\vec{e}_\theta}{r \sin \theta} \left[\frac{\partial v_r}{\partial \phi} - \sin \theta \frac{\partial}{\partial r} (r v_\phi) \right] + \frac{\vec{e}_\phi}{r} \left[\frac{\partial}{\partial r} (r v_\theta) - \frac{\partial v_r}{\partial \theta} \right].$$

Thus, the Laplacian of velocity can be expressed as

$$\Delta \vec{v} = \begin{pmatrix} \frac{1}{r} \frac{\partial^2 (r v_r)}{\partial r^2} + \frac{1}{r^2} \frac{\partial^2 v_r}{\partial \theta^2} + \frac{1}{r^2 \sin^2 \theta} \frac{\partial^2 v_r}{\partial \phi^2} + \frac{\cot \theta}{r^2} \frac{\partial v_r}{\partial \theta} - \frac{2}{r^2} \frac{\partial v_\theta}{\partial \theta} - \frac{2}{r^2 \sin \theta} \frac{\partial v_\phi}{\partial \phi} - \frac{2 v_r}{r^2} - \frac{2 \cot \theta}{r^2} v_\theta \\ \frac{1}{r} \frac{\partial^2 (r v_\theta)}{\partial r^2} + \frac{1}{r^2} \frac{\partial^2 v_\theta}{\partial \theta^2} + \frac{1}{r^2 \sin^2 \theta} \frac{\partial^2 v_\theta}{\partial \phi^2} + \frac{\cot \theta}{r^2} \frac{\partial v_\theta}{\partial \theta} - \frac{2 \cot \theta}{r^2} \frac{\partial v_\phi}{\partial \phi} + \frac{2}{r^2} \frac{\partial v_r}{\partial \theta} - \frac{1}{r^2 \sin^2 \theta} v_\theta \\ \frac{1}{r} \frac{\partial^2 (r v_\phi)}{\partial r^2} + \frac{1}{r^2} \frac{\partial^2 v_\phi}{\partial \theta^2} + \frac{1}{r^2 \sin^2 \theta} \frac{\partial^2 v_\phi}{\partial \phi^2} + \frac{\cot \theta}{r^2} \frac{\partial v_\phi}{\partial \theta} + \frac{2}{r^2 \sin \theta} \frac{\partial v_r}{\partial \phi} + \frac{2 \cot \theta}{r^2 \sin \theta} \frac{\partial v_\theta}{\partial \phi} - \frac{1}{r^2 \sin^2 \theta} v_\phi \end{pmatrix}.$$